Mineralogical Magazine, April 2006, Vol. 70(2), pp. 141–158

Formation of emeralds at pegmatite-ultramafic contacts based on fluid inclusions in Kianjavato emerald, Mananjary deposits, Madagascar

YE. VAPNIK[1], I. MOROZ[2], M. ROTH[2] AND I. ELIEZRI[3]

[1] Department of Geological and Environmental Sciences, Ben-Gurion University of the Negev, P.O.B. 653, Beer-Sheva 84105, Israel
[2] Department of Applied Physics, The Hebrew University of Jerusalem, 91904, Jerusalem, Israel
[3] Colgem El 97 Ltd, 52 Bezalel Street, Ramat Gan 52521, Israel

ABSTRACT

Kianjavato emerald (Mananjary deposits, East coast of Madagascar) was formed during metasomatic processes at the contact between pegmatites and hornblendites. The metasomatic exchange was related to a Pan-African tectonometamorphic event.

Fluid inclusions in the Kianjavato emerald and quartz were studied by means of microthermometry and Raman probe analysis. Three main types of inclusions were revealed: CO_2-rich, CH_4-rich and aqueous-rich, with a salinity of ~2 wt.% NaCl equiv. The inclusions occurred along the same primary and pseudosecondary trails and were considered to be formed simultaneously. Based on fluid-inclusion data, the conditions of emerald growth were 250ºC < T < 450ºC and P = 1.5 kbar.

The fluid inclusion data for Kianjavato emerald were compared to the data for another Madagascar emerald, Ianapera. The latter is of similar age, but its genesis was determined by a shearing event. Our fluid inclusion data suggested that shearing was also important as a mechanism of introducing CO_2-rich fluid for the genesis of the Kianjavato emerald.

KEYWORDS: fluid inclusions, Kianjavato and Ianapera emeralds, Madagascar.

Introduction

EMERALDS usually contain numerous fluid inclusion populations. Study of the inclusions allows us to characterize the composition of the fluid, its evolution and the *P-T* conditions of the emerald growth. The Kianjavato emerald grew in the most common manner of emerald growth, i.e. during metasomatic events at the boundary between pegmatites and ultramafic bodies (Schwarz, 1994). It is particularly interesting to compare the characteristics of Kianjavoto emerald with the data for another emerald from Madagascar, the Ianapera emerald (Vapnik *et al*., 2005). Both emeralds are hosted by ultrabasic bodies within Archaean gneisses. It has been suggested that the ages of formation of both types of emeralds are close, but the genesis is different (Cheilletz *et al*., 2001). There are no known pegmatite bodies in the vicinity of Ianapera, and the growth of the Ianapera emerald is related to the shearing event along the Ampanihy shear zone (Fig. 1). The present study of the Kianjavato emerald, sampled in one pit of the Mananjary emerald deposit, Madagascar, presents comprehensive new data for the fluid inclusions and emerald growth conditions.

Geological setting

The Kianjavato emerald deposit is located ~60 km west of Mananjary (Moine *et al*., 2004) on the east coast of Madagascar (Fig. 1). The Kianjavato deposit is situated in the Vohibory

* E-mail: vapnik@bgu.ac.il
DOI: 10.1180/0026461067020320

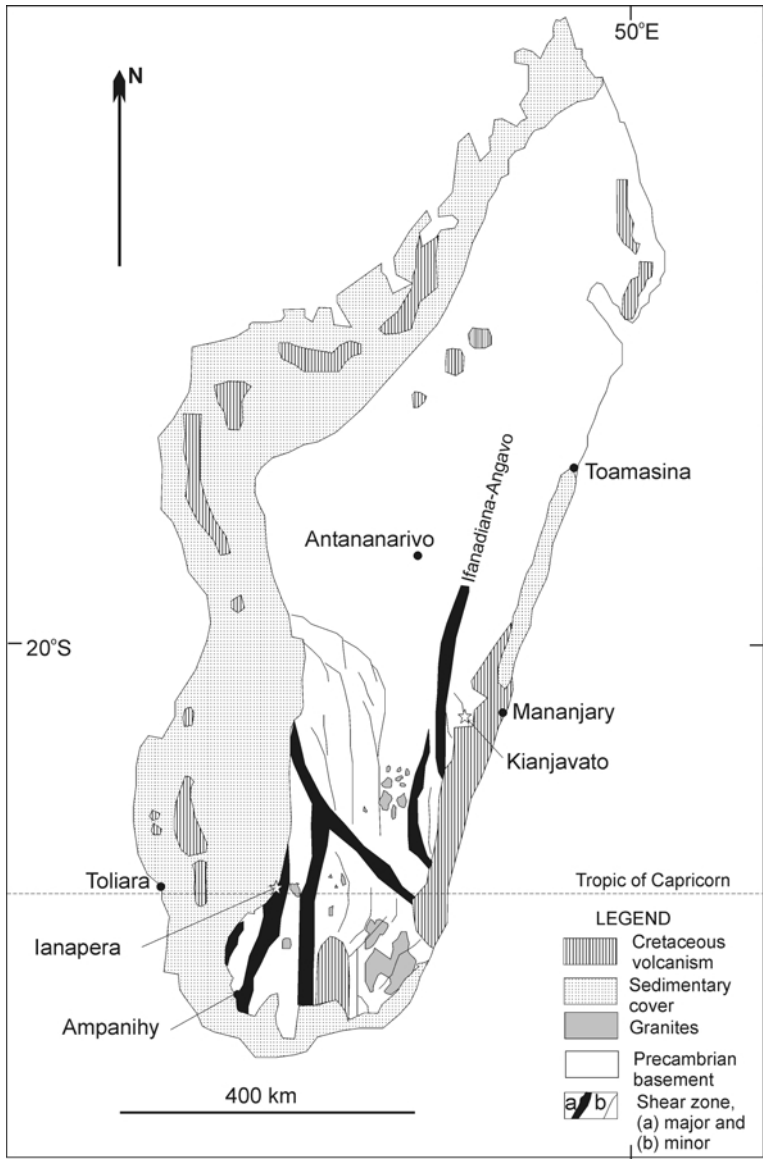

FIG. 1. General geology of Madagascar and locations of Kianjavato and Ianapera emerald deposits.

Formation which is of Precambrian age (Besairie, 1967; Nicollet, 1985). This formation consists of intermediate- to high-pressure granulite-facies rocks, which include gneisses (orthogneiss and migmatitic gneiss), leptynites, marbles, serpentinites, amphibolites (some of which are corundum-bearing) and pyroxenites. The Vohibory Formation lies conformably on the Graphite Formation in which the main petrographic feature is the abundance of graphite. This formation consists mainly of granulites and graphite gneiss (Besairie, 1967). At least two high-grade regional metamorphic and granitization events have been deduced for the area. These are a metamorphic event at 800 Ma (Handke *et al*., 1999) and a Pan-African tectonometamorphic event at 530–500 Ma (Markl *et al*., 2000). The conditions of the Pan-African metamorphism

have been determined as $P = 8\pm1$ kbar and $T = 700\pm30$ºC (Moine *et al*., 2004). Several mega-shear zones with projected lengths of >450 km and widths between 10 and 20 km extend across Madagascar. The Ifanadiana-Angavo shear zone is located to the west of the deposit, and minor related shears are probably present within the deposit area (Moine *et al*., 2004). The shear is related to compressional deformation that has been interpreted as associated with collisional events during the formation of Gondwanaland (Martelat *et al*., 1997; de Wit *et al*., 2001). The intrusion of granitic veins and pegmatites also occurred during a Pan-African event. The Precambrian lithologies are covered by recrystallized Cenozoic sedimentary rocks (mainly marbles) at their northern, western and southern margins.

The Kianjavato deposit is hosted by Archaean gneisses containing interbedded mafic (amphibolites) and ultramafic (hornblendites) bodies (Cheilletz *et al*., 2001). The emerald mineralization occurs within phlogopite-hornblende and phlogopite rocks developed at the contact between pegmatite and lenticular bodies of hornblendites. The emeralds grew in very close association with phlogopite-rich rocks, and their formation is undoubtedly related to the metasomatic processes between hornblendites and hydrothermal fluids (Moine *et al*., 2004). In this common schist-type deposit (Franz and Morteani, 2002), phlogopite-rich metasomatic bands are composed of hornblende-chlorite-phlogopite-emerald-plagioclase-calcite-quartz assemblages. Phlogopite has been dated at 490 ± 8 Ma by the $^{40}Ar/^{39}Ar$ method (Cheilletz *et al*., 2001).

Technique

To investigate inclusions, 0.1−0.2 mm thick emerald wafers, polished on both sides, were prepared. The fluid inclusions were studied at temperatures between −190 and +500ºC using the Fluid INC. heating-freezing stage. The accuracy of the temperature measurements was ~±0.5ºC in the low-temperature range (−190±50ºC) and ±2ºC in the high-temperature range (100−500ºC).

The compositions of emerald samples and their mineral inclusions were analysed using a JEOL JXA-8600 electron microprobe at the Institute of Earth Sciences of the Hebrew University of Jerusalem. This instrument was equipped with an energy-dispersive spectrometer which displayed the entire spectrum of elements (with atomic numbers of six and above) that were exposed to the focused spot of an electron beam. The microprobe was operated using a 15 kV acceleration voltage and a beam current of 10 nA. The Pioneer Norvar EDS (133 eV) computerized automation system was used to collect, store and subsequently analyse the acquired data. The standards used consisted of suitable natural minerals and synthetic materials. The detection limits for elements were generally in the range of hundreds to thousands of parts per million. As the electron microprobe spectrometer could not resolve the energies of various oxidation states of the individual elements, the total Fe content was expressed as FeO, in spite of the fact that some of the Fe in emerald could be present as Fe_2O_3 (Wood and Nassau, 1968; Platonov *et al*., 1984; Schwarz *et al*., 1996; Moroz *et al*., 1999). Vanadium may also occur in multiple valence states. The mineral formulae for the emeralds were calculated on the basis of the ideal beryl formula having 18 oxygens per formula unit. A theoretical value for BeO was computed by assuming that three Be cations were present in the beryl crystal structure.

The analysis of solid phases in fluid inclusions of emeralds was performed by use of a confocal Raman microspectrometer (Renishaw system 1000, Institute of Earth Sciences, Jerusalem) equipped with a triple monochromator and a CCD detector. The green (514.5 nm) polarized light of an argon laser beam (250 mW power) was used for excitation. The scattered light was collected through the objective ($\times 50$) of an Olympus optical microscope. Entrance slits of 100 μm gave a spectral line width of ~3.5 cm^{-1}, with a spectral resolution of <1 cm^{-1}, and a frequency reproducibility of the same order. All investigations were performed at room temperature in air. The spectral acquisition time was 30 s.

Sample characteristics

Kianjavato emeralds have a blue-green colour, range from opaque to transparent and thus resemble Zambian emeralds (Hänni and Klein, 1982; Schwarz, 1994). The results of electron microprobe analyses of several emerald crystals are shown in the Table 1. The results show that, in contrast to the Ianapera deposit gems (Vapnik *et al*., 2005), the geochemistry of emeralds from Kianjavato is characterized by small Cr_2O_3 (between 0.27 and 0.38 wt.%), V_2O_3 (0.00 and

TABLE 1. Kianjavato and Ianapera emerald composition

Sample	1	2	3	4	5	6
wt. %						
BeO	13.79	13.79	13.79	13.79	13.79	
SiO_2	62.61	61.67	61.95	62.02	61.45	63.11–64.75
Al_2O_3	14.59	14.11	14.09	14.17	14.39	10.96–14.04
MgO	2.37	2.34	2.44	2.37	2.30	1.93–3.81
Na_2O	1.53	1.16	1.17	1.69	1.68	0.42–0.93
K_2O	0.47	0.39	0.28	0.45	0.42	1.09–2.32
CaO	0.14	0.09	0.18	0.00	0.08	0.00–0.15
Cr_2O_3	0.27	0.38	0.33	0.30	0.30	0.75–3.46
TiO_2	0.08	0.26	0.00	0.07	0.00	0.00–0.07
MnO	0.00	0.00	0.02	0.00	0.00	0.00–0.13
Sc_2O_3	0.00	0.00	0.02	0.03	0.02	0.05–0.21
V_2O_5	0.00	0.00	0.03	0.00	0.00	0.00–0.47
FeO	0.96	1.26	0.96	0.88	0.95	0.65–1.82
NiO	0.18	0.10	0.00	0.00	0.07	0.00–0.43
SO_3	0.09	0.22	0.10	0.03	0.00	0.00–0.12
CoO	0.00	0.00	0.19	0.00	0.00	0.00–0.15
Rb_2O	0.00	0.00	0.00	0.00	0.00	0.00–0.50
La_2O_3	0.00	0.00	0.13	0.30	0.00	0.00–0.28
Ce_2O_3	0.00	0.24	0.40	0.00	0.00	0.00–0.34
Total	97.08	96.02	96.08	96.11	95.46	
a.p.f.u.						
Be^{2+}	3.113	3.156	3.155	3.153	3.170	
Si^{4+}	5.882	5.873	5.898	5.902	5.880	
Al^{3+}	1.616	1.583	1.581	1.589	1.622	
Mg^{2+}	0.332	0.332	0.346	0.337	0.329	
Na^{+}	0.279	0.215	0.216	0.313	0.312	
K^{+}	0.057	0.047	0.035	0.055	0.052	
Ca^{2+}	0.014	0.009	0.018	0.000	0.008	
Cr^{3+}	0.020	0.029	0.026	0.023	0.023	
Ti^{4+}	0.005	0.019	0.000	0.005	0.000	
Mn^{2+}	0.000	0.000	0.002	0.000	0.000	
Sc^{3+}	0.000	0.000	0.002	0.002	0.002	
V^{5+}	0.000	0.000	0.002	0.000	0.000	
Fe^{2+}	0.075	0.101	0.077	0.070	0.076	
Ni^{2+}	0.014	0.008	0.000	0.000	0.005	
S^{6+}	0.006	0.016	0.008	0.002	0.000	
Co^{2+}	0.000	0.000	0.014	0.000	0.000	
Rb^{+}	0.000	0.000	0.000	0.000	0.000	
La^{3+}	0.000	0.000	0.005	0.011	0.000	
Ce^{3+}	0.000	0.008	0.014	0.000	0.000	

Note: Compositions were recalculated on the basis of 3 Be and 18 O *apfu*. Samples 1–5–analyses of Kianjavato emerald; sample 6–the compositional range of Ianapera emerald.

0.03 wt.%), FeO (0.88 and 1.26 wt.%), MgO (2.30 and 2.44 wt.%), NiO (0.00 and 0.18 wt.%), CoO (0.00–0.19 wt.%), Sc_2O_3 (0.00–0.03 wt.%), La_2O_3 (0.00–0.30 wt.%), Ce_2O_3 (0.00– 0.40 wt.%) and K_2O (0.28–0.47 wt.%) contents. The emeralds do contain large amounts of Na_2O (1.16–1.69 wt.%). It should be noted that, in contrast to the Ianapera emerald (where $K_2O > Na_2O$), the Na_2O concentration in the Kianjavato emerald is three times greater than the K_2O content. The total of the oxide weight share is usually small, between 95 and 97 wt.%, which

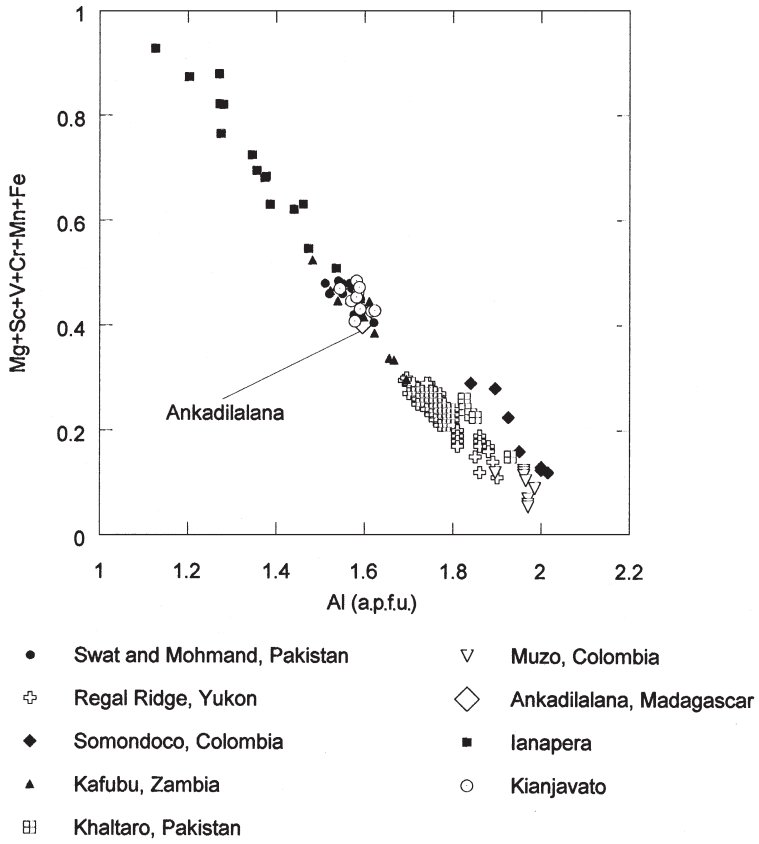

FIG. 2. Al *vs*. the sum of other *Y*-site cations, in atoms per formula unit (a.p.f.u.). The data for the Kianjavato emerald are compared with the data for Ianapera (Vapnik *et al*., 2004), Kafubu, Zambia (Seifert *et al*., 2004) and emeralds from other deposits (Groat *et al*., 2002).

is presumably mainly related to the large water content. In the chart of the negative correlation between Al and its substitutes (such as Mg, Sc, V, Cr, Mn and Fe) in the beryl structure (Fig. 2) the Kianjavato emeralds are similar to emeralds from another known deposit in the Kianjavato region Ankadilalana mine (Hänni and Klein, 1982), and emeralds from Swat and Mohmand, Pakistan (Lawrence *et al*., 1989) and Kafubu emerald, Zambia (Seifert *et al*., 2004). The ordinary (for emeralds) ratios of Mg, Fe and Cr contents make the Kianjavato emeralds similar to most other known emeralds (Fig. 3).

A large variety of mineral inclusions has been recorded in emerald by electron microprobe analysis: quartz, phlogopite, chlorite (pennine-clinochlore), talc, rutile and dolomite.

The absorption spectrum of Kianjavato emerald (Fig. 4*a*) displays a broad band at 810 nm related to Fe^{2+} ions in the octahedral Al^{3+} site, a band at 620 nm is attributed to Fe^{2+} in a channel site, an absorption edge near 400 nm is attributed to Fe^{3+} in the Al^{3+} site whereas the narrow bands at 374 nm are attributed to Fe^{3+} in Si^{4+} sites. It should be noted that the spectrum is very similar to that of Zambian emerald (Moroz *et al*., 1999). Infrared (IR) spectroscopic studies support the electron microprobe data which suggest a large amount of water in the Kianjavato emerald. The IR spectra have been obtained from powdered samples dispersed in a KBr matrix. Rather intense fundamental vibrations of H_2O molecules appear in these spectra (Fig. 4*b*). Three distinct bands are normally observed in the water-stretching modes in the range 3700–3500 cm^{-1}. The Na content, which is, on average, 1.33 wt.% for Kianjavato emerald, is the main control parameter for the intensity ratio of the bands observed. The bands

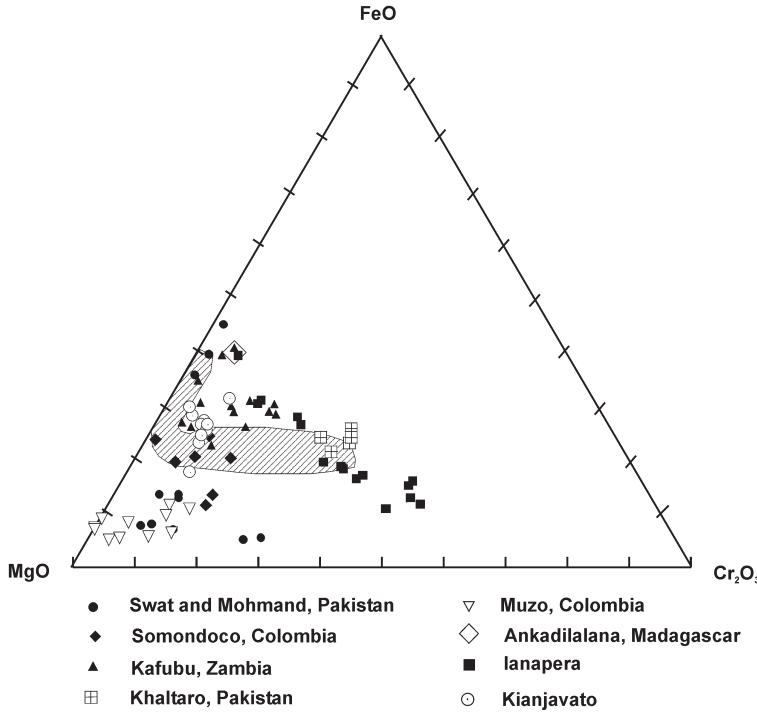

FIG. 3. Plot of emerald compositions in terms of FeO-MgO-Cr_2O_3 (wt.%). The data from this study are compared with the data for Ianapera (Vapnik *et al*., 2004), Kafubu, Zambia (Seifert *et al*., 2004) and emeralds from other deposits (Groat *et al*., 2002). The data for the Regal Ridge emerald, Yukon, are located within the hatched area.

are attributed to the presence of free water molecules (3696.1 cm^{-1} – A) and water-Na complexes (3654.3 cm^{-1} – C and 3592.7 cm^{-1} – B). The intensity ratios of the bands B > C > A are in accordance with the data of Schmetzer (1989). There are also H_2O-bending modes reflected in the presence of lines at 1635.1 and 1576.0 cm^{-1}. Rather intense vibrations of the CO_2 molecule also appear in these spectra (2357.7 cm^{-1}).

Fluid inclusion study

Fluid inclusions have been examined from several chips of emerald and emerald-hosted grains of quartz. In emerald, fluid inclusions show dispersed distribution and/or location along healed fractures. Thus, the inclusions in emerald are of primary and pseudosecondary origin. They are up to 50 μm long, commonly with negative crystal shape. In quartz, inclusions rarely show dispersed distribution and are mainly located along the linear fracture directions in many cases crossing the entire quartz grain. The inclusions in quartz are mainly of pseudosecondary/secondary origin. They are smaller than in emerald, up to 20–30 μm long. In some cases it has been observed that fractures heal with inclusions in emerald but the inclusions do not occur along the continuation of the same fracture in the quartz. Several fluid inclusion types can be observed within the same single primary or pseudosecondary inclusion population in emerald. Based on microthermometric data, the inclusions have been divided into the following types (Fig. 5): liquid and/or liquid + gaseous CO_2-rich inclusions; gaseous CH_4-rich inclusions; aqueous liquid + gaseous inclusions; mixed aqueous-CO_2 inclusions; mixed aqueous-CH_4 inclusions; mixed CO_2-CH_4 inclusions in some cases also with a visible aqueous phase. All inclusion types commonly contain single or several, usually birefringent, solid phases. The pseudosecondary/secondary inclusions in quartz are mainly represented by separate trails filled with CO_2-rich or aqueous inclusions. Nevertheless, trails exist that are also filled with CO_2-rich, aqueous and mixed CO_2-aqueous

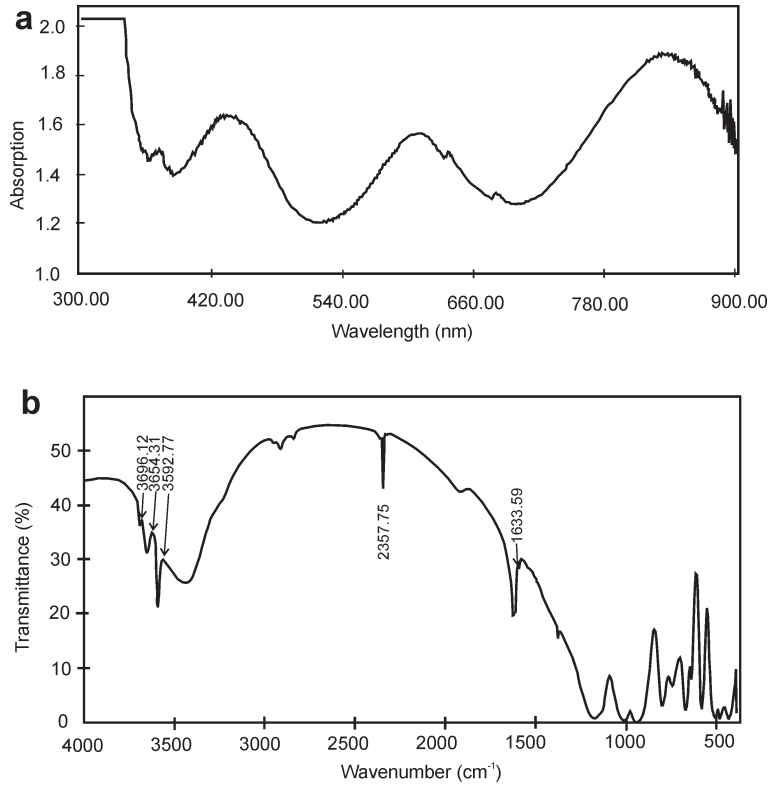

FIG. 4. Visible absorption (*a*) and IR diffuse reflectance spectra (*b*) of Kianjavato emerald at room temperature.

inclusions. Some trails are filled with small gaseous inclusions. It seems that due to the small size of these gaseous inclusions the methane-like behaviour has been observed during the freezing in one case only. Many fluid inclusions in quartz also host small birefringent solid phases.

The melting temperature (T_m) of the CO_2-rich inclusions is ~−57ºC. The range of homogenization temperatures (T_h) of CO_2 into the liquid phase is shown in Fig. 6. The primary, pseudosecondary inclusions in emerald and pseudosecondary/secondary inclusions in quartz show a similar range of T_h between 5 and 30ºC. The T_m of clathrate is observed in several inclusions at ~6.5−7.5ºC. The purity of the several CO_2-rich inclusions has been checked by the Raman probe. The spectra indicate strong CO_2 peaks with no traces of CH_4, N_2 and/or H_2S.

The aqueous inclusions in quartz and emerald show the first melting point of ice (T_{m_1}) usually in the temperature range between −8 and −4ºC (Fig. 7*a*); only in a few inclusions have T_{m_1} values as low as −18ºC have been recorded. The final melting point of ice (T_{m_f}) is usually observed between −2 and 0ºC (Fig. 7*b*). The temperature of the inclusion homogenization (liquid + gas → liquid) is between 80 and 350ºC (Fig. 7*c*), but is mainly between 150 and 290ºC. The data for aqueous inclusions are similar for inclusions hosted by quartz and emerald (Fig. 7*a,b,c*).

The data for the mixed CO_2-aqueous inclusions are shown in Fig. 8*a,b*. The T_h of CO_2 is between 6 and 31ºC (Fig. 8*a*); the visually estimated H_2O/(CO_2+H_2O) volume ratio of inclusions is between 10 and 70 vol.% (Fig. 8*b*). The clathrate melting was observed in a row of inclusions at 6.5−7.5ºC.

During cooling, the heterogenization of the gas phase is usually observed at gaseous CH_4-rich inclusions at temperatures of less than the −110 to −100ºC range. No melting phenomena have been recorded in these inclusions, whereas homogenization into the gas phase is usually observed between −85 and −78ºC; in single inclusions in emerald and quartz it has been observed at −110ºC. Within the CH_4-rich

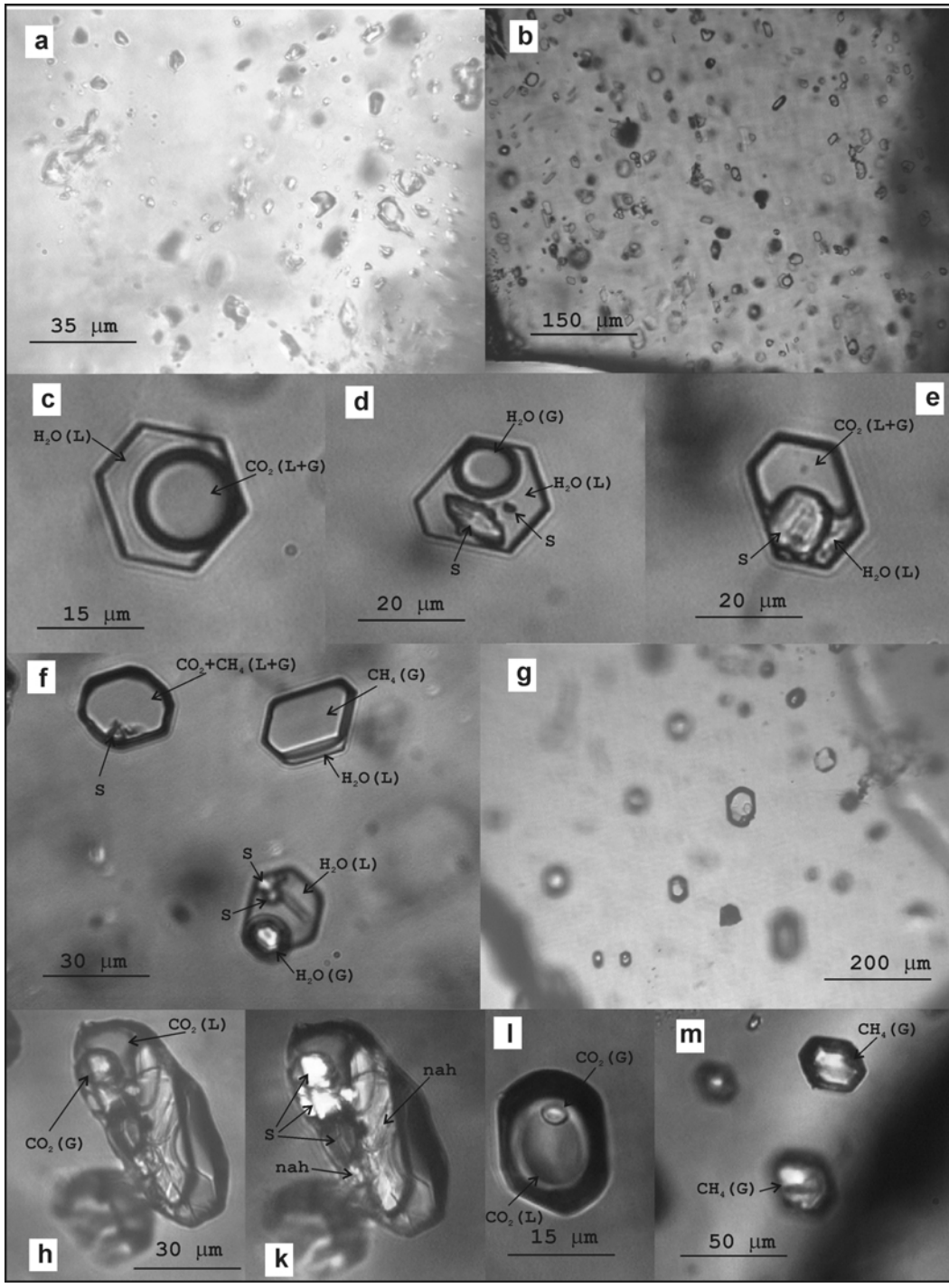
a
35 μm
b
150 μm
c
H2O (L)
CO2 (L+G)
15 μm
d
H2O (G)
H2O (L)
S
S
20 μm
e
CO2 (L+G)
S
H2O (L)
20 μm
f
CO2+CH4 (L+G)
CH4 (G)
S
H2O (L)
S
S
H2O (L)
H2O (G)
30 μm
g
200 μm
h
CO2 (L)
CO2 (G)
30 μm
k
nah
S
nah
l
CO2 (G)
CO2 (L)
15 μm
m
CH4 (G)
CH4 (G)
50 μm

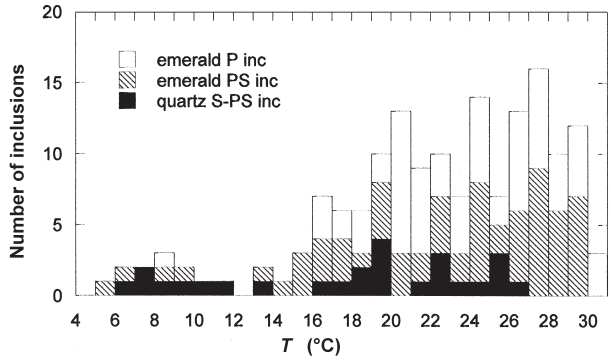

FIG. 6. Homogenization temperature (liquid + gas → liquid) of CO_2-rich inclusions. P inc, PS inc and S inc (in this and all other figures) are primary, pseudosecondary and secondary inclusions, respectively.

inclusions, the Raman probe spectra clearly feature the strong peak of CH_4; no peaks of CO_2 or other gas occur.

In the mixed CO_2-CH_4 inclusions, the first melting phenomena of solidified gases start at as low as −110ºC and, usually, the gradual melting continues up to −58ºC. The range of recorded final melting temperatures of the solidified gases is between −70 and −58ºC. The homogenization of gases is into the liquid phase within the wide temperature range of −63 to 18.5ºC. As a rule, the lowest homogenization temperature is recorded for inclusions with the lowest final melting temperatures. The Raman probe analysis reveals the peaks of CH_4 and CO_2 in these inclusions (Fig. 9*a,b*).

In some cases both CH_4-rich and mixed CO_2-CH_4 inclusions contain a visible aqueous phase; the melting of clathrate has been recorded in two cases for mixed CO_2-CH_4 inclusions at 11 and 12ºC.

All types of the above-mentioned inclusions hosted by emerald and quartz may contain a single or several solid phases. No dissolution of solid phases has ever been reported, yet nahcolite has been identified by Raman probe analysis in two inclusions. The Raman probe data (Fig. 10) indicate that calcite, Mg-calcite, magnesite and dolomite are the usual solid phases within the fluid inclusions in emerald (Burke, 1994). The solid phases in quartz were too small for Raman probe analysis. The similar types of fluid inclusions observed in quartz and emerald and the similar behaviour of solids during the heating-freezing runs in both minerals suggest that daughter phases in quartz were also composed of carbonates.

A distinct population of CO_2-rich inclusions was found in one grain of quartz. The inclusions show dispersed distribution, and they are of primary origin. These are single-phase inclusions not bearing any solid phases. The inclusions show hooked, irregular forms (Fig. 5*a*), which are typical for strongly re-equilibrated inclusions subjected to internal or confining overpressures (Sterner and Bodnar, 1989). The T_m of CO_2 is ~−57ºC, and a wide range of T_h values for CO_2 has been observed between −52 and 12ºC (Fig. 11).

Discussion

Several inclusion types are usually present within the same primary or pseudosecondary inclusion population of the Kianjavato emerald (Fig. 5). It seems that there are three main types of inclusion: CO_2-rich, CH_4-rich and aqueous inclusions, whereas other mixed inclusion types are formed by the combination of these main types.

FIG. 5. Fluid inclusions in Kianjavato emerald. (*a*) Quartz with primary super dense CO_2-inclusions. (*b*) Primary population of fluid inclusions in emerald. (c−f) Enlarged primary inclusions from the population in part *b*. (*c*) Mixed aqueous-CO_2 inclusion. (*d*) Aqueous inclusion with several solid phases. (*e*) Mixed aqueous-CO_2 inclusion with big carbonate phase. (*f*) Mixed CO_2-CH_4, mixed aqueous-CH_4, and aqueous inclusions. (*g*) Pseudosecondary population of CO_2-rich and CH_4-rich inclusions in emerald. (*h, k*) CO_2-rich inclusion hosting several carbonate and nahcolite daughter phases, uncrossed and crossed polars, respectively. (*l,m*) Enlarged CO_2-rich and CH_4-rich inclusions from the pseudosecondary population (*g*). Abbreviations L and G indicate the liquid and gas phases, respectively; S − carbonate, nah − nahcolite daughter phases.

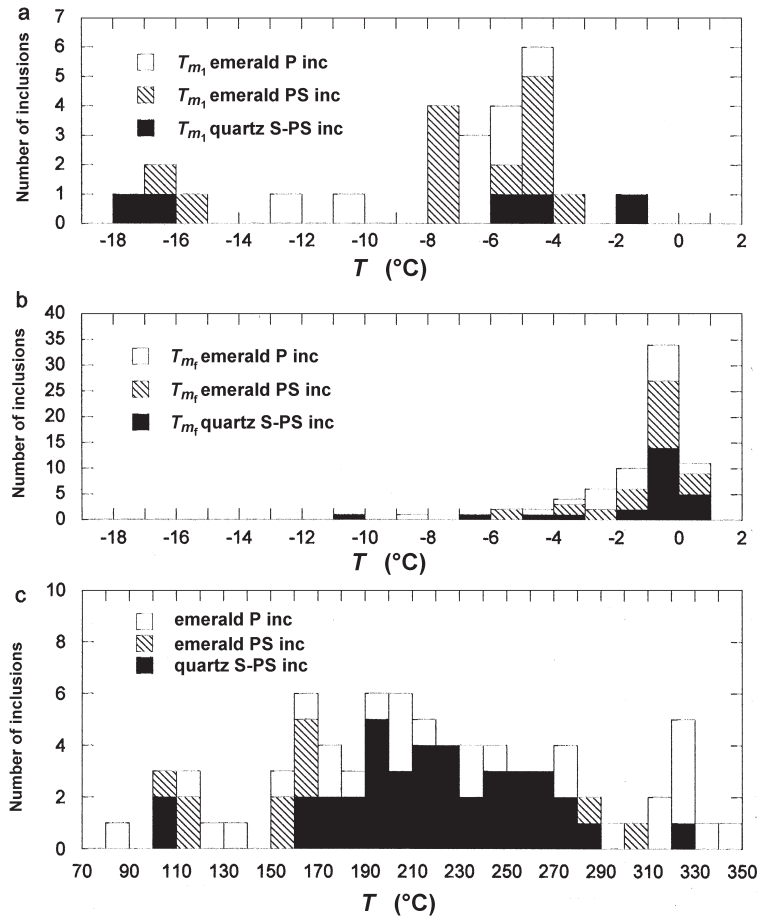

FIG. 7. Microthermometric data for aqueous inclusions: (*a*) first temperature of ice melting (T_{m_1}); (*b*) final temperature of ice melting (T_{m_f}); (*c*) homogenization temperature (liquid + gas → liquid) of aqueous inclusions.

The salinity of the aqueous inclusions is low, usually only ~1−2 wt.% NaCl equiv. Therefore, it is unlikely that fluid heterogenization is responsible for the existence of CO_2-rich (and/or CH_4-rich) and aqueous inclusions. A sequence of hydration reactions that consume H_2O, gradually enriching the residual fluid in CO_2 (Nwe and Grundmann, 1990), may describe the different CO_2/H_2O ratio in mixed aqueous-CO_2 inclusions. However, this process has also leads to the very different range of salinity of residual CO_2-H_2O inclusions, whereas the salinity of studied inclusions is always low. Mixed H_2O+CO_2±CH_4 inclusions show a similar salinity to aqueous inclusions, which clearly indicates the possibility of fluid interaction with the formation of mixed aqueous-gaseous inclusions. It seems that in the present case, the theoretical process of necking down cannot also create the observed CH_4-rich and CO_2-rich inclusions. Although CH_4 is strongly partitioned into the gas phase (Swanenberg, 1979), the possible low-temperature necking down of liquid + gas CO_2 + CH_4 inclusions with the formation of gaseous (CH_4-enriched) and liquid (CO_2-enriched) inclusions will create exclusively low-density gaseous inclusions, where CH_4 molecules would be undetectable both under the freezing and by Raman probe analysis. Thus, considering also the common primary distribution of inclusions, we suggest that all inclusion types have been formed from different but contemporaneous fluids that have existed during the emerald growth. The possibility of the existence of contemporaneous fluids is supported by isotope study. The C- and O-isotope

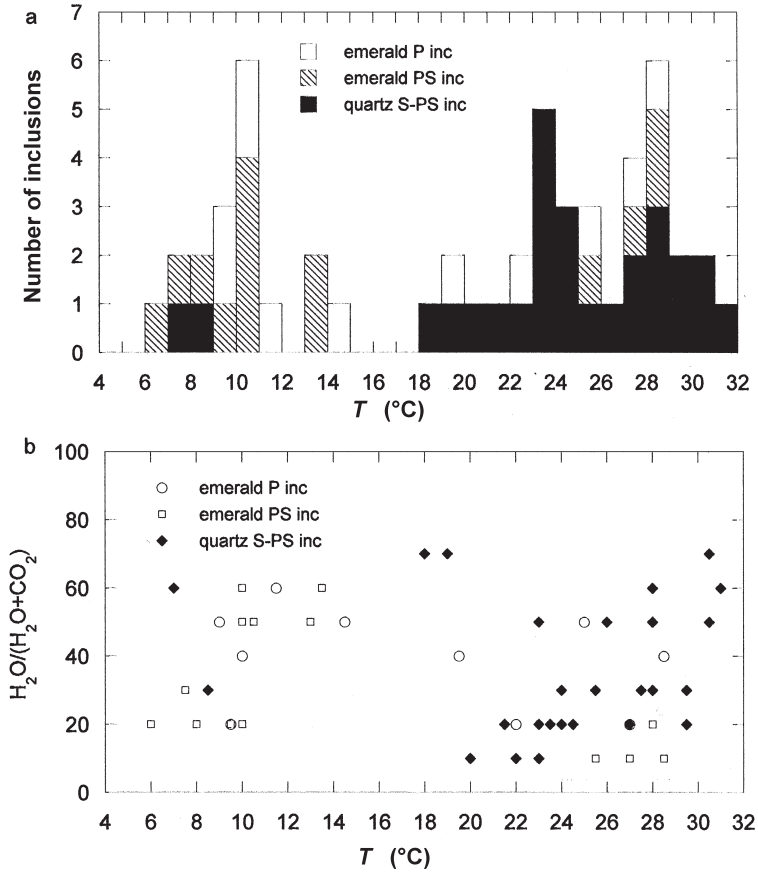

FIG. 8. Microthermometric data for mixed CO_2-aqueous inclusions: (*a*) homogenization temperature (liquid + gas → liquid) of CO_2: (*b*) $H_2O/(H_2O+CO_2)$ volume ratio of inclusions *vs.* their temperature of CO_2 homogenization.

geochemistry (Pili *et al.*, 1997) suggests that major shear zones of Madagascar, which are rooted and controlled by the mantle tend to focus mantle-derived CO_2 fluids, whereas small-scale minor shear zones, which were controlled by crustal processes, focused crustally derived H_2O-rich ± CO_2 fluids.

It is interesting to compare the fluid inclusion characteristics in the Kianjavato and Ianapera deposits (Vapnik *et al.*, 2005). Although the pattern of T_{m_1} and T_{m_f} of aqueous inclusions in the two deposits are similar, the inclusions in Ianapera emeralds show a somewhat greater salinity of up to 7 wt.% NaCl equiv. CO_2 inclusions are present in both emeralds, but the CO_2 densities are much greater for Ianapera emerald. CH_4-rich inclusions are not observed in Ianapera emerald, although oil-rich inclusions are found which is very unusual for emerald.

It seems that the discovery of CH_4-rich inclusions in Kianjavato emerald is also a very interesting phenomenon. Traces of CH_4 have been reported in several emerald deposits: Swat, Pakistan (Kazmi and Snee, 1989); Santa Terezhina, Brazil (Giuliani *et al.*, 1997), Muzo, Colombia (Ottaway *et al.*, 1994); Kafubu, Zambia (Seifert *et al.*, 2004); and Crown, Yukon (Marshall *et al.*, 2003). H_2O-CH_4 inclusions have been reported in emeralds from Spain (Fuertes-Fuente *et al.*, 2000) and Gravellote (Nwe and Morteani, 1993). As always, the source of methane is problematic, but the existence in the same inclusion of phases such as CH_4, CO_2 and H_2O suggests the equilibrium reaction between gases: $CH_4+O_2 \rightleftharpoons CO_2+H_2O$. The reaction predicts that the $CH_4/CO_2/H_2O$ ratio in fluid is related to the oxygen fugacity. The finding of pure CH_4 inclusions without traces of

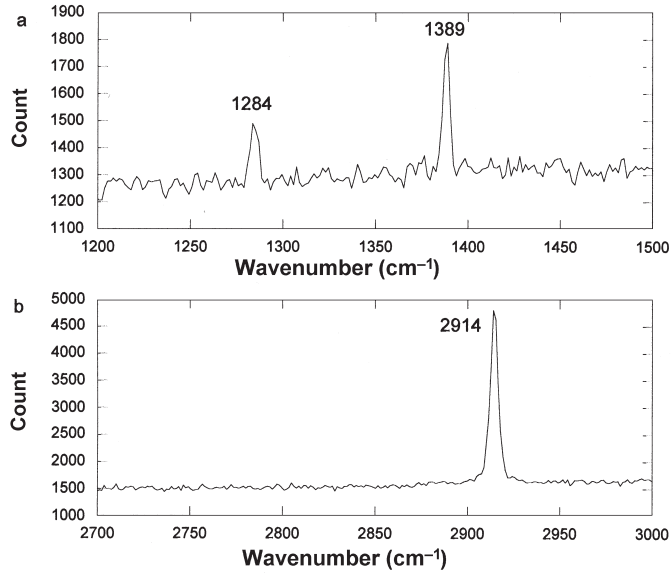

FIG. 9. Raman microspectrometry data for a mixed CO_2-CH_4 inclusion with the following microthermometric parameters: T_m final is −65ºC, and T_h is −19ºC into the liquid phase. (*a*) Spectrum of CO_2; (*b*) spectrum of CH_4.

CO_2 and H_2O phases presumes a different methane source. It has been suggested for the Ianapera emerald that the flow of CO_2-rich fluid has been promoted by deep shearing along the Ampanihy shear zone (Vapnik *et al*., 2005). It has been further suggested that the appearance of oil-bearing inclusions in Ianapera emerald is related to the reduction of this flow during the interaction with the Graphite Formation. It seems that the similar CO_2 fluid flow in the vicinity of the Ifanadiana-Angavo mega-shear zone (Fig. 1) and reduction of fluid in the graphite-rich layers, though probably in different *P-T* conditions, might have led to methane generation and trapping by Kianjavato emerald.

Primary CO_2-rich inclusions found in a single quartz grain show the characteristic forms observed for re-equilibrated inclusions (Wille and Klemd, 2004; Vapnik and Avigad, 2004); they show a wide range of densities. No such

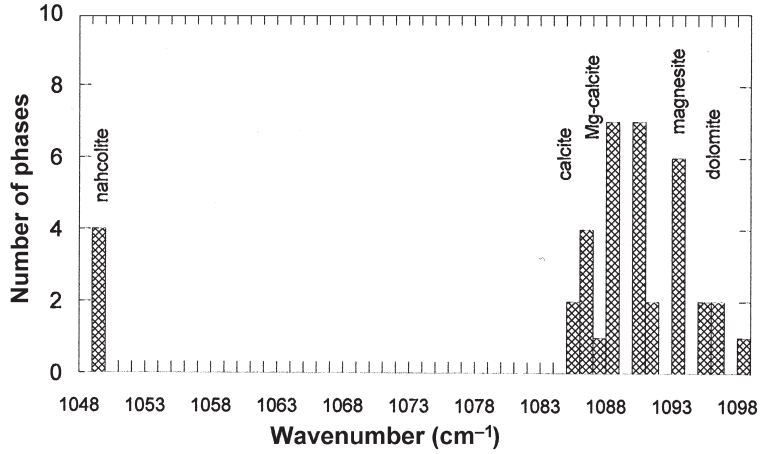

FIG. 10. Compilation of Raman data for solid daughter phases in fluid inclusions in emerald.

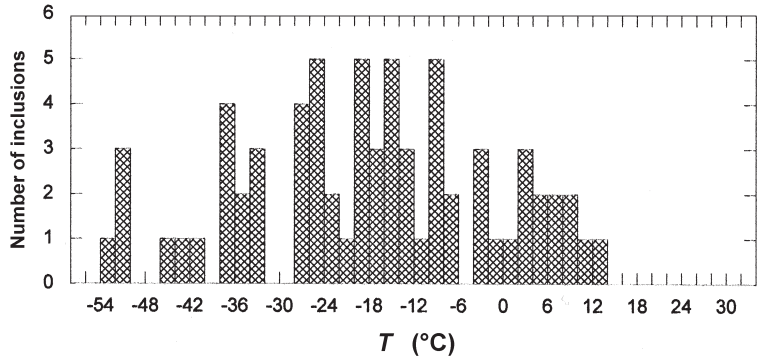

FIG. 11. Homogenization temperature (liquid + gas → liquid) of super-dense CO_2 inclusions in quartz.

inclusions were observed in any other quartz and emerald grains in the studied samples. The quartz is an unstable phase in 'blackwall zones' between quartzofeldspathic and ultramafic rocks (Franz and Morteani, 2002; Moine *et al.*, 2004) and must be mostly of post-emerald origin. The specific characteristics of fluid inclusions in this particular quartz grain suggest a relict nature for it. The suggestion that a specific quartz grain can preserve peak-condition metamorphism whereas the whole rock has suffered regressive hydrothermal alteration is not uncommon. For example, several works report contrasting fluid inclusion densities in a single or several quartz grains that correlate with the different stages of metamorphic evolution (e.g. Fonarev *et al.*, 2003).

Whereas the data for fluid inclusions in emerald are already rather numerous, the data for inclusions in quartz from emerald deposits are sparse. Based on fluid-inclusion data in quartz and emerald (Seifert *et al.*, 2004; Vapnik and Moroz, 2002) from schist-type deposits (Kafubu, Zambia, and Maria, Mozambique) and also on the paragenetic sequence of rock forming minerals (Vapnik and Moroz, 2002), early and later quartz generations with respect to emerald were specified. Rather similar data for fluid inclusions in quartz and emerald were obtained for the emerald deposit related to a shear zone – Swat, Pakistan (Seal, 1989). Nevertheless, the author suggested that the quartz post-dated the emerald (Seal, 1989). The later origin of quartz was also suggested for the deposit of problematic origin – the Sumbawanga deposit, Tanzania (Moroz *et al.*, 2001). Thus, considering mainly fluid inclusion data, it is likely that a minor part of the quartz might be a relict phase or precede the emerald crystallization, whereas most of the quartz probably formed simultaneously or followed the emerald crystallization.

The characteristics of fluid inclusions in quartz and emerald have been used to compose the possible regressive *P-T-t* path of metamorphism and evaluate the *P-T* conditions of Kianjavato emerald growth. It seems likely that the most dense CO_2 inclusion (T_h = −52ºC for CO_2) revealed in the relict quartz grain may be related to the peak metamorphic event whereas lower-density inclusions mark the inclusion re-equilibration related to decreasing *P-T* conditions. The isochore of super-dense CO_2 inclusions in relict quartz unambiguously intersects the field of *P-T* conditions evaluated for a Pan-African metamorphic event (Moine *et al.*, 2004). Most inclusions show a T_h of ~−18ºC (Fig. 11), and this isochore probably corresponds to the conditions that have provided internal overpressure and CO_2-inclusion re-equilibration (Fig. 12). The common T_h of aqueous inclusion homogenization is between 150 and 290ºC. These isochores constructed for aqueous fluid with salinity of ~2 wt.% determine the boundary conditions of the emerald growth. The CO_2 inclusions in emerald show a rather wide range of T_h between 4 and 30ºC. The comparison of the T_h (CO_2) data for CO_2-rich and mixed CO_2-aqueous inclusions shows that the quantity of inclusions with relatively low homogenization temperature is markedly increased for mixed CO_2-aqueous inclusions. Thus, it seems likely that the fluid mixing has resulted in the increase of CO_2 density. Considering this observation, more valid densities of a CO_2-rich inclusion system corresponding to T_h of 15 and 28ºC have been selected. Finally, the typical isochore of CH_4-rich inclusions, which corresponds to the methane critical

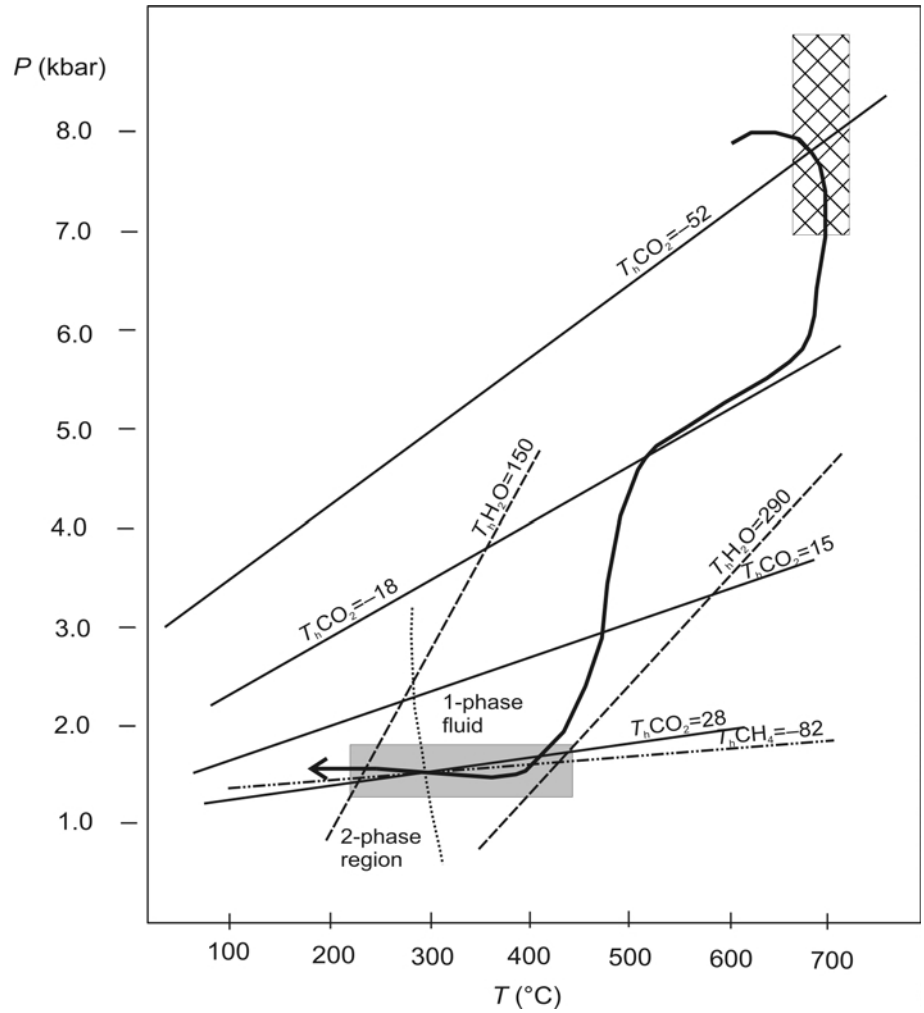

FIG. 12. The *P-T* conditions of Kianjavato emerald formation. Two isochores of super-dense CO_2 inclusions in quartz (−52) and (−18) correspond to maximal and most common densities of CO_2 inclusions. Two selected isochores of CO_2 inclusions (15) and (28), and CH_4 inclusions (−82) match the common density of CO_2 and CH_4 inclusions in emerald. The locations of CO_2 and CH_4 isochores were calculated after Belonoshko and Saxena (1991) using the software package LONER32 (Bakker, 2003). Two isochores of aqueous inclusions (150) and (290) with the salinity of 2 wt.% NaCl equiv. are constructed after Bodnar and Vityk (1994). The intersection of typical isochores of CO_2, CH_4 and aqueous inclusions determines the *P-T* field of emerald growth. The dotted line shows the *P-T* projection of CO_2-H_2O + 2 wt.% NaCl solvus (Sterner and Bodnar, 1991; Bowers and Helgeson, 1983). The upper box indicates the peak metamorphic conditions (Moine *et al*., 2004). The hatched area specifies the likely conditions of emerald growth. The bold arrow shows the suggested regressive *P-T-t* path of metamorphism.

point, has been selected. The conditions for emerald growth have been determined as the field of intersection of isochores of aqueous CO_2-rich and CH_4-rich inclusions. The conditions of the emerald growth are thus 250ºC < *T* < 450ºC, *P* = 1.5 kbar (Fig. 12). Somewhat higher *P-T* conditions of emerald growth were reported on the basis of fluid inclusion data for two coexisting fluids, aqueous and carbonic, with some mineralogical constraints taken into account (Moine *et al*., 2004). They estimated *T* up to ~500ºC and *P* up to ~2 kbar. The discrepancy is evidently

determined by the restriction superimposed by the position of the CH_4-rich inclusion isochore, which was not used in the previous study.

The estimated *P-T* field of the emerald growth intersects the solvus of the H_2O-CO_2 + 2 wt.% NaCl solution (Fig. 12). Considering mutual associations of all inclusion types in the same pseudosecondary and primary populations, inclusions have to be contemporaneous. All inclusions show similar low salinity, and thus fluid inclusion characteristics are atypical of fluid subjected to heterogenization. If the heterogenization of the fluid does not occur, then contemporaneous coexistence of carbonic-rich and aqueous fluids during the emerald growth mast be inferred. The similar two fluids also co-existed at much higher *P-T* conditions during the Ianapera emerald growth (Vapnik *et al*., 2005). The reason for non-mixing of two fluids that co-existed in the homogeneous region is unclear. It is possible that two fluids with different wetting characteristics (Brenan, 1991) may flow with different transport mechanisms, which restricts the fluid mixing.

Numerous inclusions in emerald contain carbonate solid phases, and similar birefringent phases are also numerous in similar inclusions in quartz. The carbonate and bicarbonate daughter minerals are common in emerald the growth of which involves percolation of H_2O-CO_2 fluids. The carbonate daughter minerals have been reported for several deposits (Nwe and Grundmann 1990; Giuliani *et al*., 1993; Nwe and Morteani, 1993; Giuliani *et al*., 1997; Vapnik and Moroz, 2000; Moroz *et al*., 2001; Vapnik *et al*., 2005). Nahcolite is also a common minor phase in fluid inclusions of emerald (Moroz *et al*., 2001; Vapnik *et al*., 2005), whereas in Santa Maria emeralds (Mozambique) it is the main daughter phase in fluid inclusions (Vapnik and Moroz, 2002).

Based on the microthermometric data for aqueous inclusions, namely on the data for the T_{m_1} of ice melting, and the existence of numerous carbonate phases in inclusions it is likely that the aqueous fluid is composed mainly of a Ca-Mg-Na-carbonate-bicarbonate solution with a minor Cl content. The traces of F in the fluid (up to 380 ppm) were indicated by the large F contents of phlogopite (Moine *et al*., 2004). The salinity of the aqueous phase in fluid inclusions is usually low, ~2 wt.% NaCl equiv. The solubility of Ca^{2+} is relatively low, reaching a maximum value of up to 0.025 g at T = 400ºC in the H_2O-CO_2 solution (Fein and Walther, 1987). Nevertheless, carbonate phases occupying, in some inclusions, >50% of the inclusion volume (or ~70 wt.% of the inclusion mass) are common. A simple calculation shows that the precipitation of such phases in a fluid inclusion demands the fluid/calcite volume ratio of ~10^3, if all calcite precipitates in the inclusion. It seems that experimental results may be even more realistic: the experiments suggest that the fluid/calcite volume ratio for natural vein formation may in some cases be >10^6 (Lee and Morse, 1999). In any case, it is clear that a large volume of fluid has nourished a carbonate phase during its growth in the fluid inclusion. Thus, the different volume and mass of carbonate phases in fluid inclusions may reflect the different time and different volume, respectively, of fluid that percolated through inclusions from the start to the end of their formation. We assume that the interaction with carbonic fluids promotes nucleation and precipitation of carbonates in the fluid inclusions.

Conclusions

The Kianjavato emerald originates from a geological environment that is most common for emerald growth, i.e. it was formed during a metasomatic event at the contact between pegmatite and hornblendite bodies. The clear relationship between Kianjavato emerald and pegmatites determines its chemical composition, as is the case for most other known emeralds from schist-type deposits.

The fluid inclusion study has revealed three fluid inclusion systems contemporaneous with the emerald growth: CO_2-rich, CH_4-rich and aqueous inclusions with a salinity of ~2 wt.% NaCl equiv. All inclusion types normally contain single or several daughter phases of calcite, Mg-calcite, magnesite and dolomite. Nahcolite is found in rare inclusions. Quartz hosts similar types of inclusions.

Based on microthermometric data for aqueous, CO_2 and CH_4 inclusions, the likely conditions of inclusion trapping and emerald growth have been determined. The emerald forms at 250ºC < T < 450ºC and P = 1.5 kbar.

The fluid inclusion data for Kianjavato emerald are somewhat similar to the data for another Madagascar emerald, Ianapera (Vapnik *et al*., 2005), the growth of which has been related to high-grade metamorphism and shearing. Fluid inclusions in emeralds from both deposits suggest the percolation of fluids, probably from different

sources. The CO_2-rich fluids focused in major shear zones and originated from the mantle, whereas H_2O-rich fluids were of crustal origin (Pili *et al*., 1997), i.e. these were the fluids related to pegmatite emplacement for the Kianjavato deposit. Thus, although the Kianjavato deposit is not located on the Ifanadiana-Angavo major shear zone it was suggested that fluid flow related to shearing was also important for the genesis of Kianjavato emerald. The shearing in the vicinity of the Ifanadiana-Angavo mega-shear zone probably provided the source of CO_2-rich fluid and promoted its reduction on the graphite-bearing granulites and the formation of CH_4-rich fluids.

Acknowledgements

We are obliged to O. Navon (The Hebrew University of Jerusalem) for his kind permission to use the Raman microprobe for the fluid inclusion study. We are thankful to R. Shagam (The Ben-Gurion University) for correcting the English.

References

Bakker, R.J. (2003) *Fluids 1*. Computer program for analysis of fluid inclusion data and for modeling bulk fluid properties. *Chemical Geology*, **194**, 3–23.

Belonoshko, A. and Saxena, S.K. (1991) A molecular dynamics study of the pressure-volume-temperature properties of supercritical fluids; II, CO_2, CH_4, CO, O_2 and H_2. *Geochimica et Cosmochimica Acta*, **55**, 3191–3208.

Besairie, H. (1967) The Precambrian of Madagascar. Pp. 133–142 in: *The Geologic Systems: The Precambrian* (K. Rankama, editor). Interscience 3, New York, London and Sydney.

Bodnar, R.J. and Vityk, M.O. (1994) Interpretation of microthermometric data for H_2O-NaCl fluid inclusions. Pp. 117–130 in: *Fluid Inclusions in Minerals: Methods and Applications* (B. De Vivo and M.L. Frezzotti, editors). Virginia Tech., Virginia, USA.

Bowers, T.S. and Helgeson, H.C. (1983) Calculation of the thermodynamic and geochemical consequences of nonideal mixing in the system H_2O-CO_2-NaCl on phase relations in geological systems: Equation of state for H_2O-CO_2-NaCl fluids at high pressures and temperatures. *Geochimica et Cosmochimica Acta*, **47**, 1247–1275.

Brenan, J. (1991) Development and maintenance of metamorphic permeability: Implication for fluid transport. Pp. 291–319 in: *Contact Metamorphism* (D.M. Kerrick, editor). Reviews in Mineralogy, **26**. Mineralogical Society of America, Washington, D.C.

Burke, E.A.J. (1994) Raman microspectrometry of fluid inclusions: The daily practice. Pp. 25–44 in: *Fluid Inclusions in Minerals: Methods and Applications* (B. De Vivo and M.L. Frezzotti, editors). Virginia Tech., Virginia, USA.

Cheilletz, A., Sabot, B., Marchand, P., De Donato, P., Taylor, B., Archibald, D., Barres, O. and Andrianjaffy, J. (2001) Emerald deposits in Madagascar: Two different types for one mineralizing event. EUG XI, Symposium OSO6, Abstracts, p. 547.

de Wit, M.J., Bowring, S.A., Ashwal, L.D., Randrianasolo, L.G., Morel, V.P.I. and Rambeloson, R.A. (2001) Age and tectonic evolution of Neoproterozoic ductile shear zones in Southwestern Madagascar, with implications for Gondwana studies. *Tectonics*, **20**, 1–45.

Fein, J.B. and Walther, J.V. (1987) Calcite solubility in supercritical CO_2-H_2O fluids. *Geochimica et Cosmochimica Acta*, **51**, 1665–1673.

Fonarev, V.I., Santosh, M., Vasiukova, O.V. and Filimonov, M.B. (2003) Fluid evolution and exhumation path of the Trivandrum Granulite Block, southern India. *Contributions to Mineralogy and Petrology*, **145**, 339–354.

Franz, G. and Morteani, G. (2002) Be-minerals: Synthesis, stability, and occurrence in metamorphic rocks. Pp. 551–590 in: *Beryllium: Mineralogy, Petrology, and Geochemistry* (E.S. Grew, editor). Reviews in Mineralogy and Geochemistry, **50**, Mineralogical Society of America, Washington, D.C.

Fuertes-Fuente, M., Martin-Izard, A., Boiron, M.C. and Viñuela, J.M. (2000) P-T path and fluid evolution in the Franqueira granitic pegmatite, central Galicia, northwestern Spain. *The Canadian Mineralogist*, **38**, 1163–1175.

Giuliani, G., Cheilletz, A., Dubessy, J. and Rodriguez, C. T. (1993) Chemical composition of fluid inclusions in Colombian emerald deposits. Pp. 159–168 in: *Proceedings of the Eighth Quadrennial IAGOD Symposium.*

Giuliani, G., Cheilletz, A., Zimmermann, J.-L., Ribeiro-Althoff, A.M., France-Lanord, C. and Féraud, G. (1997) Les gisements d'émeraude du Brésil: genèse et typologie. *Chronique de la Recherche Minière*, **526**, 17–61.

Groat, L.A., Marshall, D.D., Giuliani, G., Murphy, D.C., Piercey, S.J., Jambor, J.J., Mortensen, J.K., Ercit, T.S., Gault, R.A., Mattey, D.P., Schwarz, D., Maluski, H., Wise, M.A., Wengzynowski, W. and Eaton, D.W. (2002) Mineralogical and geochemical study of the Regal Ridge emerald showing, southeastern Yukon. *The Canadian Mineralogist*, **40**, 1313–1338.

Handke, M.J., Tucker, R.D. and Ashwal, L.D. (1999)

Neoproterozoic continental arc magmatism in west-central Madagascar. *Geology*, **27**, 351–354.

Hänni, H.A. and Klein, H.H. (1982) Ein smaragdvorkommen in Madagaskar. *Zeitschrift der Deutschen Gemmologischen Gesellschaft*, **31**, 71–77.

Kazmi, A.H. and Snee, L.W. (1989) Geology of world emerald deposits: a brief review. Pp. 165–228 in: *Emeralds of Pakistan: Geology, Gemmology and Genesis* (A.H. Kazmi and L.W. Snee, editors). Van Nostrand Reinhold publishers, The Netherlands.

Lawrence, R.D., Kazmi, A.H. and Snee, L.W. (1989) Geological setting of the emerald deposits. Pp. 13–38 in: *Emeralds of Pakistan: Geology, Gemmology and Genesis* (A.H. Kazmi and L.W. Snee, editors). Van Nostrand Reinhold publishes, The Netherlands.

Lee, Y.-J. and Morse, J.W. (1999) Calcite precipitation in synthetic veins: implications for the time and fluid volume necessary for vein filling. *Chemical Geology*, **156**, 151–170.

Markl, G., Baeuerle, J. and Grujic, D. (2000) Metamorphic evolution of Pan-African granulite facies metapelites from southern Madagascar. *Precambrian Research*, **102**, 47–68.

Marshall, D., Groat, L., Giuliani, G., Murphy, D., Mattey, D., Ercit, T.S., Wise, M.A., Wengzynowski, W. and Eaton, W.D. (2003) Pressure, temperature and fluid conditions during emerald precipitation, southeastern Yukon, Canada: fluid inclusion and stable isotope evidence. *Chemical Geology*, **193**, 187–199.

Martelat, J.E., Nicollet, C., Lardeaux, J.M., Vidal, G. and Rarotondrazafy, R. (1997) Lithospheric tectonic structures developed under high-grade metamorphism in the southern part of Madagascar. *Geodinamika Acta*, **10**, 94–114.

Moine, B., Chan Peng, C. and Mercier, A. (2004) Rôle du fluor dans la formation des gisements d'émeraude de Mananjary (Est de Madagascar). *Comptes Rendus Geosciences*, **336**, 513–522.

Moroz, I., Roth, M. and Deich, V. (1999) The visible absorption spectroscopy of emeralds from different deposits. *The Australian Gemmologist*, **20**, 315–320.

Moroz, I., Vapnik, Ye., Eliezri, I. and Roth, M. (2001) Mineral and fluid inclusion study of emeralds from the Lake Manyara and Sumbawanga deposits, Tanzania. *Journal of African Earth Sciences*, **33**, 377–390.

Nicollet, C. (1985) The banded cordierite and garnet-bearing gneisses from Ihosy: a geothermo-barometric tracer in southern Madagascar. *Precambrian Research*, **28**, 175–185.

Nwe, Y.Y. and Grundmann, G. (1990) Evolution of metamorphic fluids in shear zones: The record from the emeralds of Habachtal, Tauern Window, Austria. *Lithos*, **25**, 281–304.

Nwe, Y.Y. and Morteani, G. (1993) Fluid evolution in the H_2O-CH_4-CO_2-NaCl system during emerald mineralization at Gravelotte, Murchison Greenstone Belt, Northeast Transvaal, South Africa. *Geochimica et Cosmochimica Acta*, **57**, 89–103.

Ottaway, T.L., Wicks, F.J., Bryndzia, L.T., Kyser, T.K. and Spooner, E.T.C. (1994) Formation of the Muzo hydrothermal emerald deposit in Colombia. *Nature*, **369**, 552–554.

Pili, É., Ricard, Y., Lardeaux, J.-M. and Sheppard, S.M.F. (1997) Lithospheric shear zones and mantle-crust connections. *Tectonophysics*, **280**, 15–29.

Platonov, A.N., Taran, M.N. and Balitsky, V.S. (1984) *Nature of Gem Colors*. Nedra, Moscow, 205 pp. (in Russian).

Schmetzer, K. (1989) Types of water in natural and synthetic emerald. *Neues Jahrbuch für Mineralogie, Monatshefte*, 15–26.

Schwarz, D. (1994) Emeralds from the Manajary region, Madagascar: Internal features. *Gems and Gemology*, **30**, 88–101.

Schwarz, D., Kanis, J. and Kinnaird, J. (1996) Emerald and green beryl from Central Nigeria. *Journal of Gemmology*, **25**, 117–141.

Seal, R.R. II (1989) A reconnaissance study of the fluid inclusion geochemistry of the emerald deposits of Pakistan and Afghanistan. Pp. 152–164 in: *Emeralds of Pakistan: Geology, Gemology and Genesis* (A.H. Kazmi and L.W. Snee, editors). Van Nostrand Reinhold publishers, The Netherlands.

Seifert, A.V., Žáček, V., Vrána, S., Pecina, V., Zachariás, J. and Zwaan, J.C. (2004) Emerald mineralization in the Kafubu area, Zambia. *Bulletin of Geosciences*, **79**, 1–40.

Sterner, S.M. and Bodnar, R.J. (1989) Synthetic fluid inclusions VII. Re-equilibration of fluid inclusions in quartz during laboratory simulated metamorphic burial and uplift. *Journal of Metamorphic Geology*, **7**, 243–260.

Sterner, S.M. and Bodnar, R.J. (1991) Synthetic fluid inclusions. X: Experimental determination of P-V-T-X properties in the CO_2-H_2O system to 6 kb and 700ºC. *American Journal of Sciences*, **291**, 1–54.

Swanenberg, H.E.C. (1979) Phase equilibria in carbonic systems, and their application to freezing studies of fluid inclusions. *Contributions to Mineralogy and Petrology*, **68**, 303–306.

Vapnik, Ye. and Avigad, D. (2004) P-T conditions of quartz-calcite boudins and vein formation within a low-angle detachment fault in Tinos Island (Aegean Sea): a fluid-inclusion study. *International Journal of Earth Sciences*, **93**, 487–499.

Vapnik, Ye. and Moroz, I. (2000) Fluid inclusions in emerald from the Jos complex (Central Nigeria). *Schweizerisch Mineralogische Petrographische Mitteilungen*, **80**, 117–129.

Vapnik, Ye. and Moroz, I. (2001) Fluid inclusions in Panjshir emerald (Afghanistan). Pp. 451–454 in: *ECROFI XVI* (F. Noronha, A. Dória and A. Guedes, editors). Abstracts. Porto, Portugal.

Vapnik, Ye. and Moroz, I. (2002) Composition and formation conditions of fluid inclusions in emerald from Maria deposit (Mozambique). *Mineralogical Magazine*, **66**, 201–213.

Vapnik, Ye., Sabot, B. and Moroz, I. (2005) Fluid inclusions in Ianapera emerald, Southern Madagascar. *International Geology Review*, **47**, 647–662.

Wille, S.E. and Klemd, R. (2004) Fluid inclusion studies of the Abawso gold prospect, near the Ashanti Belt, Ghana. *Mineralium Deposita*, **39**, 31–45.

Wood, D.L. and Nassau, K. (1968) The characterization of beryl and emerald by visible and infrared absorption spectroscopy. *The American Mineralogist*, **53**, 777–800.

[*Manuscript received 5 July 2005: revised 7 February 2006*]